Identifying intermediates in the reductive intramolecular cyclisation of allyl 2-bromobenzyl ether by an improved electron paramagnetic resonance spectroelectrochemical electrode design combined with density functional theory calculations

Identifying intermediates in the reductive intramolecular cyclisation of allyl 2-bromobenzyl ether by an improved electron paramagnetic resonance spectroelectrochemical electrode design combined with density functional theory calculations

Danny Pauwels[a], H. Y. Vincent Ching[b], Mohammad Samanipour[b], Sander Neukermans[a], Jonas Hereijgers[a], Sabine Van Doorslaer[b], Karolien De Wael[c], Tom Breugelmans[a]*

[a] *University of Antwerp, Research Group Advanced Reactor Technology, Universiteitsplein 1, 2610 Wilrijk, Belgium.*

[b] *University of Antwerp, Laboratory of Biophysics and Biomedical Physics, Universiteitsplein 1, 2610 Wilrijk, Belgium.*

[C] *University of Antwerp, Research Group Antwerp X-ray analysis, Electrochemistry and Speciation, Groenenborgerlaan 171, 2020 Antwerp, Belgium.*

**Corresponding Author: tom.breugelmans@uantwerpen.be*

Abstract

The electrochemical activation of C-X bonds requires very negative electrode potentials. Lowering the overpotentials and increasing the catalytic activity requires intensive electrocatalytic research. A profound understanding of the reaction mechanism and the influence of the electrocatalyst allows optimal tuning of the electrocatalyst. This can be achieved by combining electrochemical techniques with electron paramagnetic resonance (EPR) spectroscopy. Although this was introduced in the mid-twentieth century, the application of this combined approach in electrocatalytic research is underexploited. Several

reasons can be listed, such as the limited availability of EPR instrumentation and electrochemical devices for such in situ experiments. In this work, a simple and inexpensive construction adapted for in situ EPR electrocatalytic research is proposed. The proof of concept is provided by studying a model reaction, namely the reductive cyclisation of allyl 2-bromobenzyl ether which has interesting industrial applications.

Keywords

Spectroelectrochemistry; EPR; electrosynthesis; cyclisation; DFT

1. Introduction

The electrosynthetic reduction of organic halides has attracted extensive interest and accompanying research [1,2]. This interest has been sparked by the many important applications associated with these reactions, such as reduction of environmental pollutants, investigation of the DET (dissociative electron transfer) mechanism, carbon fixation and upgrading of organics through activation of the R-X bond [3–7]. Of specific interest is the synthesis of heterocyclic compounds due to important applications in pharmaceuticals [8–10], pesticides [11], dyes [12] and synthetic applications [13].

An industrially relevant and interesting case is the cyclisation of allyl 2-bromobenzyl ether to 4-methylisochromane (a benzopyran derivate). On the one hand, it is considered a model reaction [14,15] and, on the other hand, it is of importance for the pharmaceutical industry as benzopyran is an essential building block for numerous drugs. Conventional synthesis of heterocycles is complex and requires a large number of reaction steps and the use of auxiliaries which results in a low selectivity [2]. As a viable alternative, electrosynthesis

offers many advantages such as fewer steps, milder reaction conditions, higher selectivity, less pollutants and waste streams, and avoids the need of expensive or hazardous reagents [16–18]. The reductive radical cyclisation of aryl halides onto an unsaturated bond is frequently used to construct fused aromatics in heterocyclic organic synthesis [14,19]. However, a major drawback of using organic halides in electrosynthesis is that the electrochemical activation of C-X bonds, especially in chlorides and bromides, requires very negative electrode potentials, which is impractical for industrial production processes due to exuberant energy costs. To reduce the large overpotentials and increase selectivity, research has been directed towards improving the catalytic activity of the electrode materials [20–23]. The strategies that have been employed include: investigating different bulk materials that have shown potential for the carbo-halogen bond rupture such as Ag, Pd, Ni and Cu [21,24–26], tuning the morphology and geometrical characteristics of the electrode [22,27], and using a homogeneous electrocatalysis route with mainly transition-metal complexes [14,28–31]. In order to select the best electrocatalytic material and optimally tune the catalysts, a profound knowledge of the complex reaction mechanism and the effect of the catalyst is required. Figure shows a proposed mechanism for the cyclisation of allyl 2-bromobenzyl ether [23].

<FIGURE 1>

The reduction of aryl halides occurs through a dissociative electron transfer leading to the scission of the carbon-halogen bond [6,24]. There are two possible pathways for this: a stepwise mechanism or a concerted mechanism. The former is shown by reaction (1) and (2) with the formation of an intermediate radical anion, the latter is presented by reaction (3)

leading directly to the allyl benzyl ether radical. This radical can then undergo an intramolecular cyclisation reaction (4) after which it is reduced (5). Alternatively, the allyl benzyl ether radical can also be reduced directly (6). Since the product of interest is the benzopyran derivate obtained in reaction (5), the optimization of the electrocatalyst will also include preventing reaction (6) from taking place.

Being able to detect and identify these radicals during the reaction, will provide essential information on the chemical nature and electronic structure of the different intermediates and the influence of the catalyst. A technique which is capable of this, is electron paramagnetic resonance (EPR). EPR is a spectroscopic technique that uses the electron as a probe to infer information of paramagnetic species, such as organic radicals. Since radicals are the predominant species generated during electrosynthesis, a platform for combined EPR and electrochemical experiments would be of particular use. The first experiments in which electrochemical research and EPR have been combined date from well over half a century ago [32,33]. Since then, a lot of research has been conducted in this field together with development of the necessary equipment and set-ups [34–36]. Several different electrode and cell designs, both static and in flow regime for in situ spectroelectrochemical EPR research have been reported [37]. Most often a set-up to identify radicals generated in electrochemical reactions utilizes a common EPR TE_{102} cavity and standard flat cell in combination with a simple electrode design such as the laminated mesh electrode proposed by Neudeck *et al*. [38]. Despite the advances during the last decades, the use of such combined platform remains underexploited in the field of electrocatalytic research. Reasons for this include EPR being less widely available than most other spectroscopic instrumentations, and the necessary electrochemical devices being complex and delicate, and have generally been home-made. In this work, a set-up is constructed for combined in situ

EPR and electrochemical experiments. The set-up is based on a previous design, but optimized for versatility and applicability in electrocatalyst research. This requires design features which are not provided by cells reported in literature. An important aspect is that the working electrode has a flat surface to incorporate nanostructured catalysts in the combined in situ experiments. As the substrate has a substantial influence on the deposited electrocatalysts, it is of importance that the electrode surface is highly reproducible and offers a similar performance between different experiments. Additionally, often multiple repeated experiments are performed, so the design should be simple and inexpensive. To have a broad applicability the set-up should be suitable for both aqueous and non-aqueous environments. Lastly, it should display reasonably defined electrochemical behavior for accurate electrolysis of complex reactions. As a proof of concept, we describe here our investigation of the intermediates in the reductive cyclisation of allyl 2-bromobenzyl ether, which to the best of our knowledge, has not been reported in the literature. The scope is not to achieve a complete understanding of the electrocatalytic mechanism of this reaction on silver, but to demonstrate the usefulness of this methodology in electrocatalytic research and to confirm the general scheme of the cyclisation reaction investigated.

2. Experimental

2.1. Chemicals

Acetonitrile (ACN, HPLC gradient grade, ≥99.9 %) was purchased from Chem-Lab (Belgium). Allyl 2-bromobenzyl ether (ABBE, 95 %), (2,2,6,6-tetramethylpiperidin-1-yl)oxyl (TEMPO), the spin trapping agent *N*-tert-Butyl-α-phenylnitrone (PBN, for ESR-spectroscopy, ≥99.5 %) and the supporting electrolyte tetrabutylammonium perchlorate (n-Bu_4NClO_4, 99.0 %) were purchased from Sigma-Aldrich (Belgium).

2.2. Set-up and procedure

The combined EPR and electrochemical experiments were performed in a Wilmad WG-810 Suprasil® (quartz) electrolytic flat cell. The cell was positioned in a TE102 cavity in a Bruker E580 Elexsys spectrometer and a custom-constructed electrode was used (Figure 2).

<FIGURE 2>

This electrode is based upon the original Adams cell [39] from which many different designs have emerged, usually employing a metal mesh or foil as working electrode. In this work, a 200 nm film of the target working electrode material was coated onto a 30 µm polypropylene substrate by means of sputter deposition. The geometrical surface area of the electrode was 4 mm^2. This provides a reproducible flat working electrode surface which is tunable in size and geometry. In addition only a very small amount of metal is brought into the active part of the cavity, so the EPR signal is not significantly disturbed. As reference electrode a Teflon coated 75 µm diameter Ag wire was fixed to the substrate and stripped near the working electrode leading to a very small distance between both (<1 mm). This short distance results in an acceptable uncompensated resistance. A Pt wire wound around the electrode's base acts as a counter electrode and was positioned directly above the flat part of the cell. This set-up with a sputter-coated working electrode provides a simple, inexpensive and flexible platform for combined EPR and electrochemistry measurements (Figure 2). It was validated in both aqueous and non-aqueous environments using the reduction of methyl viologen and the reduction of benzoquinone as standard reactions (results shown in Figure S1 in the supporting information). In both cases, the setup gave a good voltammetric response (i.e. the

expected response with a similar peak shape to a batch measurement on a planar electrode) and the expected EPR spectra of the generated radicals could be obtained.

Experimental solutions were prepared with 0.1 M n-Bu_4NClO_4, 5 mM of the analyte and 15 mM of PBN. Prior to measurements, the solutions were extensively flushed with argon. To fill the cell, approximately 1.5-2 ml is pipetted under inert atmosphere. The filled cell is further flushed with argon, creating an argon blanket on top of the solution. The cell is closed by inserting the electrode construction from the top and is then transferred to the spectrometer and connected to the potentiostat. A PAR VersaSTAT 3 is used to apply and measure the electrochemical signal. Firstly, CVs are measured to determine the exact potential of the reduction peak versus the pseudo-reference electrode in this cell. Then the experiment is performed by applying a constant potential set at the cathodic peak potential. The EPR spectra are recorded simultaneously at X-band in continuous-wave (CW) mode (~9.7 GHz) at room temperature with 5 mW microwave power 0.1 mT modulation amplitude and 100 kHz modulation frequency.

2.3. EPR simulations and density functional theory (DFT) calculations

The EPR spectra were simulated using the EasySpin-5.1.11 module [40] running in Matlab 2017a. Spin-unrestricted (UKS) DFT computations were performed with the ORCA package [41–44] for PBN-Ox, PBN-allyl benzyl ether and PBN-4-methylisochromane in ACN, and TEMPO, and (5,5-dimethyl-2-hydroxyl-pyrrolin-1-yl)oxyl (DMPO-OH) in water. To simulate the solvent effect, a dielectric surrounding with the dielectric constant of the respective solvents according to the COSMO model was used [45]. For the geometry optimizations, the Becke-Perdew density functional (BP86) [46–48] and the split-valence plus polarization (SVP) basis set [49] were used for all atoms. The energy was converged to

1×10^{-8} Hartree (Eh) and the convergence tolerances in the geometry optimization were 3×10^{-4} Eh/Bohr for the gradient and 5×10^{-6} Eh for the total energy. The coordinates of the optimized geometries are given in Table S2. For benchmarking, single-point calculations with the B3LYP/EPR-II, B3LYP/6-31+G**, and PWPB95/EPR-II functional/basis sets [50–53] were used to predict the EPR spectral parameters form the optimized geometries.

3. Results and discussion

3.1. Electrochemical validation

In previous work from our laboratory [23], several cathode materials were investigated as potential electrocatalyst for the electrochemical cyclisation of allyl 2-bromobenzyl ether to 4-methyl-3,4-dihydro-1*H*-2-benzopyran (4-methylisochromane) and an activity scale of bulk materials was determined. It was shown that out of the selected materials, silver exhibits the best activity with a very high selectivity towards the product of interest. It was also shown that on silver, two distinct reduction waves were observable, corresponding with one or two electrons being transferred. Setting the potential to the first reduction peak (least negative potential) exclusively yields 4-methylisochromane, while at the second reduction peak the major product is the undesired allyl benzyl ether (((allyloxy)methyl)benzene). Since 4-methylisochromane is the desired product, the reaction at the first reduction peak will be investigated.

An electrode was constructed as described in section 2.2 with Ag as the working electrode material. A CV study was performed to find the potential of the reduction peak versus the pseudo-reference electrode. This was done in both a standard batch set-up and in the EPR flat cell so electrochemical behavior of the electrode in both situations could be compared (Figure 3 A and B). Both voltammograms clearly show the reduction peak with a slight shift

of the peak potential in the flat cell. The flat compartment of the spectroscopic cell wherein the working electrode resides is ≤250 µm and entails a high ohmic drop (see Figure 2), hence the shift is to be expected. However, due to the very thin electrode thickness of ~30 µm, semi-infinite linear diffusion is approximated and the response is less distorted than previous electrochemical measurements in cells of similar dimensions [54]. The peak shapes of both voltammograms are also comparable, but the peak in the flat cell experiment is slightly less pronounced and more spread out as a consequence of the diffusion limitations. The voltammogram in the flat cell shows a good response which allows identifying the peaks and deriving the peak potential. The presence of PBN in the electrolyte gave a comparable voltammogram which has a slightly changed shape as a result of the kinetic influences due to the interference of the spin trap with the mechanism. This is not an issue in the bulk electrolysis experiments as PBN itself is not electroactive in the potential window of the measurements [55]. We want to stress that, in many literature reports, in situ voltammograms are omitted or show strong distortion [56–58], which renders it difficult or impossible to correctly identify peaks and peak potentials. In such cases, the batch data are often used, but this does not necessary accurately reflect the situation in the in situ cell. The electrode construction as presented here shows good performance but is also simple.

<FIGURE 3>

3.2. In situ *EPR electrochemical study of the cyclisation reaction*

Using the in situ setup, potential-controlled electrolysis experiments with simultaneously EPR measurements were performed on samples containing allyl 2-bromobenzyl ether in ACN with *n*-Bu_4NClO_4. However, no EPR signals were observed, most probably due to the

high reactivity of the radical intermediates in the proposed mechanism (Figure 1) such that they did not accumulate to detectable concentrations. Consequently, PBN was introduced in excess to the experiments as a spin-trap. Spin-traps react with short-living radicals and convert them to more stable, EPR-detectable radical species.

The current response of the experiment is shown in Figure 4. In the first quarter of the total experiment time up until 1800 s, the current is rather unstable, slowly increasing over time and exhibiting some peaks towards more negative currents. At first sight, this appears random, but repeated experiments under the same conditions confirmed that this is reproducible and thus, can be linked to the processes taking place. It is suggested that the pseudo-random course in the first 1800 s is due to the setup transitioning into a steady state. Due to the thin geometry of the cell and the relatively large bulk, this happens much slower than in a standard batch cell. After about 2700 s the current more or less stabilizes, after which the current slightly decreases. It is known that Br^- resulting from the C-X bond cleavage can adsorb onto Ag, blocking the surface [59]. However, this is only effective at potentials less negative than -1.2 V vs. SCE. Since the exact potential during the electrolysis cannot be determined due to the changes in the environment of the pseudo-reference, it is not possible to definitively assign the fluctuation to this event. A decreasing current as seen from 2700 s onwards can be expected, even at steady state electrolysis.

<FIGURE 4>

In correlation with the current response, a change in the CW-EPR spectrum over time is also observed. The scans were accumulated over a time period of 30 min or 20 scans at four points during the experiment (marked by the dashed lines in Figure 4). 20 scan accumulations were chosen due to the poor signal-to-noise (S/N) of the initial spectra, and

this was maintained for consistency. Clear changes in the spectral features over time can be observed in the CW-EPR spectra (normalized) (Figure 5). In the corresponding unnormalized spectra (Figure 6) an increase in the signal intensities over time is also observed. Also depicted in Figure 6, is the unnormalized spectrum of a potential controlled electrolysis experiment on a solution containing only PBN in ACN with *n*-Bu_4NClO_4 after 75 min. In this control experiment a small EPR signal of an unknown radical is also observed, but it was not present in the allyl 2-bromobenzyl ether experiments.

<FIGURE 5>

Table 1: Experimental and calculated isotropic *g* and hyperfine coupling constants of the three spin-trapped radicals during the electrolysis of 5 mM ABBE + 15 mM PBN in ACN + 0.1 M TBAP (potential set at the peak potential of the reduction wave in the EPR flat cell, checked by in situ CV).

	radical 1		**radical 2**		**radical 3**	
	exp	*cal*	*exp*	*cal*	*exp*	*cal*
g_{iso}	2.0069	2.0067	2.0063	2.0053	2.0062	2.0054
$A_{N\text{-}iso}$ [MHz]	22.66	22.53	39.09	40.35	39.53	43.17
A_H^{β} [MHz]	-	-	6.46	5.61	12.43	12.18
A_H [MHz]	-	-	-	-	4.03	1.43 (A_{H2}^{φ})/ -0.82 ($A_{H_a}^{\gamma}$)/ -0.94 ($A_{H_b}^{\gamma}$)[a]
A_H [MHz]	-	-	-	-	2.19	

[a] Possible assignments (see main text for details)

As the changes in features and amount of splitting in the spectra suggests, all spectra are convoluted spectra of more than one species. All spectra agree with the features expected for nitroxide radicals formed by trapping of a reactive organic radical with PBN [60].The formed nitroxide radicals have a longer lifetime than the original radicals, which decayed

too fast to be detected with CW EPR. The spectra can be interpreted in terms of an isotropic *g* value and the hyperfine interactions (*A*) between the unpaired electron and the magnetic nuclei in its vicinity. These parameters can be used as a unique fingerprint of the trapped radical. Due to the interaction of the unpaired electron with the nitroxide ^{14}N nucleus (I=1), the room-temperature CW-EPR spectra of all nitroxide radicals consist of at least a triplet signal. Subsequent splitting of the three signals can occur through resolved hyperfine interaction with protons in the vicinity of the unpaired electron. The spectrum depicted in Figure 5A is a sum of a triplet (radical 1) and a triplet of doublets (radical 2). In the following spectrum, Figure 5B, the contribution of a third species emerges (radical 3). The EPR features of radical 3 are more pronounced in the third (Figure 5C) and fourth (Figure 5D) spectrum. All EPR spectra can be simulated in terms of these three contributions (Figure 5) for which the parameters are listed in Table 1. From the simulations, the EPR spectrum of radical 3 was found to be a triplet of doublets of doublets of doublets. The individual EPR contributions are shown in Figure 5E-G.

<FIGURE 6>

Based on the isotropic ^{14}N hyperfine coupling constant (22.66 MHz) of radical 1, it is assigned to benzoyl-*tert*-butyl nitroxide (PBN-Ox) (Figure 5) [60]. This species is often observed in PBN spin-trapping experiments, especially in the presence of oxygen [61]. Although the electrolyte was extensively deoxygenated during sample preparation and was under an argon atmosphere during the experiment, there still can be residual dioxygen in the electrolyte due to its high solubility in ACN (8.1 mM [62]). Alternatively, residual water in the ACN solvent (<150 ppm) can be oxidized at the counter electrode and the generated

dioxygen can diffuse to the working electrode part of the cell. Radicals 2 and 3, displayed ^{14}N and ^{1}H hyperfine couplings that are suggestive of carbon-centered radicals that have been spin-trapped such as the expected radical intermediates from reactions (3) and (4) in Figure 1. In order to assign radicals 2 and 3, DFT was used to compute the EPR parameters of the PBN spin-trapped allyl benzyl ether and 4-methylisochromane radicals. The computational method (appropriate choice of basis sets and functionals) was benchmarked using standard nitroxide radicals TEMPO ((2,2,6,6-tetramethylpoperidin-1-yl)oxyl), and 5,5-dimethyl-1-pyrroline *N*-oxide (DMPO)-OH as well as PBN-Ox (see table S1). All three functional/basis sets that were tested reasonably predicted the g_{iso} values. The B3LYP/(6-31+G**) was found to be most accurate for calculating the hyperfine interactions (Figure S2), and thus was chosen for calculating the EPR parameters of the spin-trap radicals. Variations between different functional/basis sets and deviations from the exact experimental values are normal for DFT computations, but the observed trends are generally followed [63].The geometry-optimized models of PBN-Ox, PBN-allyl benzyl ether, and PBN-4-methylisochromane are depicted in Figure 5. Compared to PBN-Ox, the latter two PBN-adducts have greater degrees of freedom. To account for this, selected bonds close to the nitroxide moiety were manually rotated. Rotation around the N-C^{β} bond had the most significant impact on the EPR parameters calculated from the molecular models (Figure S3). Averaging the values of the thermally allowed (kT = 25.7 meV at 298 K) N-C^{β} bond rotamers, yielded EPR parameters for PBN-4-methylisochromane and PBN-allyl benzyl ether that are comparable to radical 2 and 3, respectively (table 1), and thus are assigned accordingly. The calculations reasonably predicted the g_{iso} values for both radicals. For radical 2, the experimental and calculated hyperfine coupling values are in good agreement (Table 1). These are assigned to the expected isotropic ^{14}N interaction, and the interactions

between the unpaired electron and the H^{β} proton (see Figure 5 for proton assignment). For radical 3, the experimental and calculated values for the isotropic ^{14}N and H^{β} proton hyperfine interactions are also in good agreement. Two further ^{1}H interactions (4.03 and 2.19 MHz) are also used in the simulation of the spectrum of radical 3. After the isotropic ^{14}N and H^{β} proton, the next largest calculated hyperfine interactions are $H2^{\varphi}$ (1.43 MHz), $A_{H_b}{}^{\gamma}$ protons (-0.94 MHz) and $A_{H_a}{}^{\gamma}$ (-0.82 MHz). Two of these are likely candidates for the unattributed couplings in the spectrum of radical 3. However, the calculated values are close in magnitude and somewhat smaller than the experiment preventing definitive assignments.

As shown in Figure 5, the three PBN-trapped radicals are not all present at each time interval. The relative weight of each radical in the spectrum correlates linearly with their relative concentration and can be plotted versus the elapsed time to visualize their evolution (Figure 7). The presence of the PBN-Ox increases with time then plateaus, suggesting that the electrolytic generation of this species is exhaustive, or that it reaches steady-state between PBN-Ox decay and spin-trapping reactions. Considering the very low concentration of residual oxygen/water, exhaustive electrolysis is plausible. The concentration of PBN-allyl benzyl ether appears to decrease between the first and second time intervals. This change is small and maybe due to the poor S/N of the first spectrum. Considering the few data points, it is assumed that this decrease is insignificant within the experimental error. From the second time interval to the remainder of the experiment the concentration of PBN-allyl benzyl ether remains constant. PBN-4-methylisochromane, which arises from the spin-trapping of the radical intermediate from the intramolecular cyclisation of the allyl benzyl ether radical is the most abundant product over time. This is expected as the experimental

conditions favored its formation. There is strong increase in the concentration of PBN-4-methylisochromane in the beginning which starts to plateaus in the last time interval.

<FIGURE 7>

The data suggests that the cyclisation intermediate (4-methylisochromane radical) is not present during the first time interval, which is unexpected considering the precursor intermediate (allyl benzyl ether radical) is formed. However, it should be noted that the intermediates are not detected directly, and that an extra spin-trapping reaction step is needed for detection. The reactivity of PBN with different radicals can vary [64] and thus the formation of certain radicals can be masked. It is possible that PBN-Ox is formed much more easily than PBN-4-methylisochromane. Alternately, the 4-methylisochromane radical generated is reacting with the fast diffusing residue oxygen in the initial stages, which yields PBN-Ox after subsequent decay/reaction steps. Due to the geometry of the thin cell, natural convection quickly sets in. Over time the oxygen species becomes exhausted and more of the target radical will be spin-trapped and becomes detectable in the spectra. This appears to follow the course of the current in Figure where after the first time interval, the current starts to stabilize (no longer strongly influenced by the oxygen/water species), after which PBN-4-methylisochromane emerges in the subsequent spectra. In addition, the S/N is lower in the beginning, possibly masking the spectral features of a low amount of the PBN-4-methylisochromane. This correlates with the previous results of a electrochemical investigation [23] which shows that product distribution is not time dependent and that the cyclisation product is formed at any point during the electrolysis. The concentration of the allyl benzyl ether radical remains almost constant throughout the electrolysis while the

concentration of the 4-methylisochromane radical increases. This implies that the intramolecular cyclisation to 4-methylisochromane is faster or easier than the spin-trapping reaction. A possible cause is the difference in adsorption strength of the radicals. The allyl benzyl ether radical could be strongly adsorbed on the surface while the 4-methylisochromane radical is more easily desorbed due to the cyclisation which breaks the Ag-radical bond. Since the trapping reaction with PBN happens in solution the 4-methylisochromane will undergo this more easily resulting in a larger concentration of trapped radicals. Furthermore the decomposition of the trapped radicals plays a role. The stability of the trapped radicals may be different for the different adducts which can lead to differences in the accumulated concentrations. A less stable radical reaches a steady state concentration much faster.

4. Conclusions

Employing a platform for combined EPR and electrochemical measurements to elucidate mechanisms remains underexploited in electrocatalytic research. In this work this approach is validated on a model reaction and for the first time, the proposed mechanism for the reductive cyclisation of allyl 2-bromobenzyl ether to 4-methylisochromane was confirmed. Both the allyl benzyl ether radical and the 4-methylisochromane radical intermediates could be detected by spin-trapping and identified with the help of DFT calculations. As expected, the target cyclic radical was the most abundant product. To this end, a simple, inexpensive and versatile electrode set-up for in situ EPR and electrochemical experiments has been constructed. The set-up is suitable for both aqueous and non-aqueous environments and shows both a good electrochemical as a good EPR response and can be used in an EPR flat cell in a TE_{102} cavity. These results show the strength of combined EPR and electrochemical

measurements in electrocatalytic research. Currently we are developing a similar set-up for flow-cell experiments to expand the applicability of the platform. A flow-cell will allow deriving kinetic information such as the radical decay rates and offers an increased sensitivity for short-lived radicals. The cell design is based on a channel electrode [65] which is adapted to fulfill the requirements to incorporate nanostructured electrocatalysts, similar to the set-up in this work. We are also exploring the possibility of adapting the set-up for rapid-scan EPR methods [66,67] which will greatly decrease the acquisition time and thus improve the detection sensitivity of the set-up.

Acknowledgements

The authors would like to thank Melissa Van Landeghem for her assistance with the experimental work and analysis of the data. Jonas Hereijgers greatly acknowledges the Research Foundation - Flanders (FWO) for support through a Post-Doctoral grant (12Q8817N). H. Y. Vincent Ching gratefully acknowledges the University of Antwerp for a Post-Doctoral grant. Sabine Van Doorslaer and Tom Breugelmans acknowledge the FWO for research funding (research grant G093317N).

References

[1] H.J. Schäfer, Contributions of organic electrosynthesis to green chemistry, Comptes Rendus Chim. 14 (2011) 745–765. doi:10.1016/j.crci.2011.01.002.

[2] E. Duñach, M. José Medeiros, S. Olivero, Intramolecular reductive cyclisations using electrochemistry: development of environmentally friendly synthetic methodologies, New J. Chem. 30 (2006) 1534–1548. doi:10.1039/B608228A.

[3] C. Durante, B. Huang, A.A. Isse, A. Gennaro, Electrocatalytic dechlorination of volatile organic compounds at copper cathode. Part II: Polychloroethanes, Appl. Catal. B Environ. 126 (2012) 355–362. doi:10.1016/j.apcatb.2012.07.003.

[4] C. Durante, V. Perazzolo, A.A. Isse, M. Favaro, G. Granozzi, A. Gennaro, Electrochemical Activation of Carbon-Halogen Bonds: Electrocatalysis at Palladium-Copper Nanoparticles, ChemElectroChem. 1 (2014) 1370–1381. doi:10.1002/celc.201402032.

[5] C. Durante, A.A. Isse, G. Sandonà, A. Gennaro, Electrochemical hydrodehalogenation of polychloromethanes at silver and carbon electrodes, Appl.

Catal. B Environ. 88 (2009) 479–489. doi:10.1016/j.apcatb.2008.10.010.
[6] A.A. Isse, S. Gottardello, C. Durante, A. Gennaro, Dissociative electron transfer to organic chlorides: electrocatalysis at metal cathodes., Phys. Chem. Chem. Phys. 10 (2008) 2409–2416. doi:10.1039/b719936h.
[7] D.F. Niu, L.P. Xiao, A.J. Zhang, G.R. Zhang, Q.Y. Tan, J.X. Lu, Electrocatalytic carboxylation of aliphatic halides at silver cathode in acetonitrile, Tetrahedron. 64 (2008) 10517–10520. doi:10.1016/j.tet.2008.08.093.
[8] M.M. Burbuliene, V. Jakubkiene, G. Mekuskiene, E. Udrenaite, R. Smicius, P. Vainilavicius, Synthesis and anti-inflammatory activity of derivatives of 5-[(2-disubstitutedamino-6-methyl-pyrimidin-4-yl)-sulfanylmethyl]-3H-1,3,4-oxadiazole-2-thiones, Farm. 59 (2004) 767–774. doi:10.1016/j.farmac.2004.05.007.
[9] L. Pieters, S. Van Dyck, M. Gao, R. Bai, E. Hamel, a Vlietinck, G. Lemière, Synthesis and biological evaluation of dihydrobenzofuran lignans and related compounds as potential antitumor agents that inhibit tubulin polymerization., J. Med. Chem. 42 (1999) 5475–5481. doi:10.1021/jm990251m.
[10] H.F. Roaiah, S.S. El-Nakkady, W.S. El-Serwy, M.A.A. Ali, A.H.A. El-Rahman, Z. El-Bazza, Studies on some benzopyran derivatives with expected antimicrobial and antiviral activity, Nat. Sci. 8 (2010) 20–29.
[11] E. Ayranci, N. Hoda, Adsorption kinetics and isotherms of pesticides onto activated carbon-cloth, Chemosphere. 60 (2005) 1600–1607. doi:10.1016/j.chemosphere.2005.02.040.
[12] A.S. Shawali, Synthesis and tautomerism of aryl- and hetaryl-azo derivatives of bi- and tri-heterocycles, J. Adv. Res. 1 (2010) 255–290. doi:10.1016/j.jare.2010.07.002.
[13] K.C. Majumdar, G. V. Karunakar, B. Sinha, Formation of five- and six-membered heterocyclic rings under radical cyclization conditions, Synth. 44 (2012) 2475–2505. doi:10.1055/s-0032-1316566.
[14] E. Duñach, A.P. Esteves, M.J. Medeiros, C.S. dos Santos Neves, S. Olivero, Radical-type reactions in protic and aprotic media: Comparisons in nickel-catalysed electrochemical reductive cyclisations, Comptes Rendus Chim. 12 (2009) 889–894. doi:10.1016/j.crci.2008.09.025.
[15] E. Duñach, A.P. Esteves, A.M. Freitas, M.J. Medeiros, S. Olivero, Electroreductive cyclisation of unsaturated halides catalysed by nickel macrocyclic complexes, Tetrahedron Lett. 40 (1999) 8693–8696.
[16] R. Francke, R.D. Little, Redox catalysis in organic electrosynthesis: basic principles and recent developments, Chem. Soc. Rev. 43 (2014) 2492–2521. doi:10.1039/c3cs60464k.
[17] H. Lund, O. Hammerich, Organic Electrochemistry, 4th ed., Marcel Dekker, Inc., 1991.
[18] D. Pletcher, F.C. Walsh, Industrial Electrochemistry, 2nd ed., Chapman and Hall, London, 1990.
[19] W.R.L. and L.D.R. Sowell C.G., Electroreductive cyclization reaction, stereoselectino creation of quaternary centres in bicyclic frameworks and a formal total synthesis of quadrone, Tetrahedron Lett. 31 (1990) 95–98.
[20] V. Jouikov, J. Simonet, The one-electron cleavage of benzylic bromides at palladium and palladized cathodes: Benzyl radicals generation and immobilization onto solid interfaces, Electrochem. Commun. 12 (2010) 331–334. doi:10.1016/j.elecom.2009.12.009.
[21] C. Bellomunno, D. Bonanomi, L. Falciola, M. Longhi, P.R. Mussini, L.M. Doubova,

G. Di Silvestro, Building up an electrocatalytic activity scale of cathode materials for organic halide reductions, 50 (2005) 2331–2341. doi:10.1016/j.electacta.2004.10.047.
[22] B. Geboes, B. Vanrenterghem, J. Ustarroz, D. Pauwels, S. Sotiropoulos, A. Hubin, T. Breugelmans, Influence of the morphology of electrodeposited nanoparticles on the activity of organic halide reduction, 2014. doi:10.3303/CET1441013.
[23] B. Vanrenterghem, T. Breugelmans, An activity scale of cathode materials for the electrochemical cyclisation of allyl 2-bromobenzyl ether, Electrochim. Acta. 234 (2017) 28–36. doi:10.1016/j.electacta.2017.03.016.
[24] A.A. Isse, G. Berzi, L. Falciola, M. Rossi, P.R. Mussini, A. Gennaro, Electrocatalysis and electron transfer mechanisms in the reduction of organic halides at Ag, J. Appl. Electrochem. 39 (2009) 2217–2225. doi:10.1007/s10800-008-9768-z.
[25] P. Poizot, J. Simonet, Silver-palladium cathode: Selective one-electron scission of alkyl halides: Homo-coupling and cross-coupling subsequent reactions, Electrochim. Acta. 56 (2010) 15–36. doi:10.1016/j.electacta.2010.09.020.
[26] J. Simonet, The one-electron reduction of primary alkyl iodides at palladium and palladiated surfaces: a facile source of alkyl radicals?, Electrochem. Commun. 7 (2005) 74–80. doi:10.1016/j.elecom.2004.10.006.
[27] B. Vanrenterghem, B. Geboes, S. Bals, J. Ustarroz, A. Hubin, T. Breugelmans, Influence of the support material and the resulting particle distribution on the deposition of Ag nanoparticles for the electrocatalytic activity of benzyl bromide reduction, Appl. Catal. B Environ. 181 (2016) 542–549. doi:10.1016/j.apcatb.2015.08.026.
[28] A.P. Esteves, A.M. Freitas, M.J. Medeiros, D. Pletcher, Reductive intramolecular cyclisation of unsaturated halides by Ni(II) complexes, J. Electroanal. Chem. 499 (2001) 95–102. doi:10.1016/S0022-0728(00)00494-0.
[29] X. Chaminade, E. Duñach, A.P. Esteves, M.J. Medeiros, C.S. Neves, S. Olivero, Electrosynthesis of nitrogen heterocycles using environmentally friendly methodologies, Electrochim. Acta. 54 (2009) 5120–5126. doi:10.1016/j.electacta.2009.01.004.
[30] S. Olivero, J.C. Clinet, E. Duñach, Electrochemical intramolecular reductive cyclisation catalysed by electrogenerated Ni(cyclam)2+, Tetrahedron Lett. 36 (1995) 4429–4432. doi:10.1016/0040-4039(95)00782-8.
[31] E. Duñach, a. P. Esteves, M.J. Medeiros, D. Pletcher, S. Olivero, The study of nickel(II) and cobalt(II) complexes with a chiral salen derivative as catalysts for the electrochemical cyclisation of unsaturated 2-bromophenyl ethers, J. Electroanal. Chem. 566 (2004) 39–45. doi:10.1016/j.jelechem.2003.10.045.
[32] D.E.G. Austen, P.H. Given, D.J.E. Ingram, M.E. Peover, Electron Resonance Study of the Radicals Produced by Controlled Potential Electrolysis of Aromatic Substances, Nature. 182 (1958) 1784–1786. doi:10.1038/1821784a0.
[33] A.H. Maki, D.H. Geske, Detection of Electrolytically Generated Transient Free Radicals by Electron Spin Resonance, J. Chem. Phys. 30 (1959) 1356. doi:10.1063/1.1730187.
[34] A.J. Bard, L.R. Faulkner, Electrochemical methods: Fundamentals and Applications, 2nd ed., John Wiley & Sonc, Inc., 2001.
[35] R.J. Gale, Spectroelectrochemistry, theory and practice, Plenum Press, New York, 1988.
[36] P.T. Kissinger, W.R. Heineman, Laboratory techniques in electroanalytical

chemistry, 2nd ed., Marcel Dekker, Inc., 1996.
[37] R.D. Webster, A.M. Bond, B.A. Coles, R.G. Compton, ESR-electrochemical cells: A comparative study, J. Electroanal. Chem. 404 (1996) 303–308. doi:10.1016/0022-0728(95)04363-2.
[38] A. Neudeck, L. Kress, Laminated micro-meshes - A new kind of optically transparent electrode, J. Electroanal. Chem. 437 (1997) 141–156. http://www.scopus.com/inward/record.url?eid=2-s2.0-0031269541&partnerID=40&md5=fd05526d829ea0eb3ebd1da86de205ca.
[39] L.H. Piette, P. Ludwig, R.N. Adams, Electron Paramagnetic Resonance and Electrochemistry. Studies of Electrochemically Generated Radical Ions in Aqueous Solution., Anal. Chem. 34 (1962) 916–921. doi:10.1021/ac60188a013.
[40] S. Stoll, A. Schweiger, EasySpin, a comprehensive software package for spectral simulation and analysis in EPR, J. Magn. Reson. 178 (2006) 42–55. doi:10.1016/j.jmr.2005.08.013.
[41] F. Neese, Prediction of electron paramagnetic resonance g values using coupled perturbed Hartree-Fock and Kohn-Sham theory, J. Chem. Phys. 115 (2001) 11080–11096. doi:10.1063/1.1419058.
[42] F. Neese, Theoretical Study of Ligand Superhyperfine Structure. Application to Cu(II) Complexes, J. Phys. Chem. A. 105 (2001) 4290–4299. doi:10.1021/jp003254f.
[43] F. Neese, Metal and ligand hyperfine couplings in transition metal complexes: The effect of spin-orbit coupling as studied by coupled perturbed Kohn-Sham theory, J. Chem. Phys. 118 (2003) 3939–3948. doi:10.1063/1.1540619.
[44] F. Neese, Efficient and accurate approximations to the molecular spin-orbit coupling operator and their use in molecular g-tensor calculations, J. Chem. Phys. 122 (2005). doi:10.1063/1.1829047.
[45] S. Sinnecker, A. Rajendran, A. Klamt, M. Diedenhofen, F. Neese, Calculation of solvent shifts on electronic g-tensors with the conductor-like screening model (COSMO) and its self-consistent generalization to real solvents (direct COSMO-RS), J. Phys. Chem. A. 110 (2006) 2235–2245. doi:10.1021/jp056016z.
[46] J.P. Perdew, Density-functional approximation for the correlation energy of the inhomogeneous electron gas, Phys. Rev. B. 33 (1986) 8822–8824.
[47] J.P. Perdew, Erratum: Density-functional approximation for the correlation energy of the inhomogeneous electron gas, Phys. Rev. B. 34 (1986) 7406.
[48] A.D. Becke, Density-functional exchange-energy approximation with correct asymptotic behavior, Phys. Rev. A. 38 (1988) 3098–3100. doi:10.1103/PhysRevA.38.3098.
[49] A. Schäfer, H. Horn, R. Ahlrichs, Fully optimized contracted Gaussian basis sets for atoms Li to Kr, J. Chem. Phys. 97 (1992) 2571–2577.
[50] P.J. Stephens, F.J. Devlin, C.F. Chabalowski, M.J. Frisch, Ab Initio Calculation of Vibrational Absorption and Circular Dichroism Spectra Using Density Functional Force Fields, J. Phys. Chem. 98 (1994) 11623–11627. doi:10.1021/j100096a001.
[51] D. Moran, A.C. Simmonett, F.E. Leach, W.D. Allen, P.V.R. Schleyer, H.F. Schaefer, Popular theoretical methods predict benzene and arenes to be nonplanar, J. Am. Chem. Soc. 128 (2006) 9342–9343. doi:10.1021/ja0630285.
[52] L. Goerigk, S. Grimme, Efficient and accurate double-hybrid-meta-GGA density functionals- evaluation with the extended GMTKN30 database for general main group thermochemistry, kinetics, and noncovalent interactions, J. Chem. Theory Comput. 7 (2011) 291–309. doi:10.1021/ct100466k.

[53] V. Barone, Structure, Magnetic properties and Reactivities of Open-Shell Species from Density Functional and Self-Consistent Hybrid Methods, in: D.P. Chong (Ed.), Recent Adv. Density Funct. Methods, 1st ed., World Scientific, 1995: pp. 287–334.
[54] I.B. Goldberg, A.J. Bard, S.W. Feldberg, Resistive Effects in Thin Electrochemical Cells: Digital Simulations of Electrochemistry in Electron Spin Resonance Cells, J. Phys. Chem. 76 (1972) 2550–2559.
[55] G.L. McIntire, H.N. Blount, H.J. Stronks, R. V. Shetty, E.G. Janzen, Spin trapping in electrochemistry. 2. Aqueous and nonaqueous electrochemical characterizations of spin traps, J. Phys. Chem. 84 (1980) 916–921. doi:10.1021/j100445a026.
[56] G. Armendáriz-Vidales, C. Frontana, Insights into dissociative electron transfer in esterified shikonin semiquinones by in situ ESR/UV-Vis spectroelectrochemistry, Phys. Chem. Chem. Phys. 17 (2015) 29299–29304. doi:10.1039/C5CP04306A.
[57] R.T. Boeré, A.M. Bond, T. Chivers, S.W. Feldberg, T.L. Roemmele, Identification of the Radical Anions of C 2 N 4 S 2 and P 2 N 4 S 2 Rings by In Situ EPR Spectroelectrochemistry and DFT Calculations, Inorg. Chem. 46 (2007) 5596–5607. doi:10.1021/ic070243t.
[58] L. Ignatovich, V. Jouikov, Organogermatranes and their cation radicals by EPR-spectroelectrochemistry and ab initio calculations, J. Organomet. Chem. 751 (2014) 546–554. doi:10.1016/j.jorganchem.2013.08.007.
[59] T. Wandlowski, J.X. Wang, B.M. Ocko, Adsorption of bromide at the Ag(100) electrode surface, J. Electroanal. Chem. 500 (2001) 418–434. doi:10.1016/S0022-0728(00)00380-6.
[60] G.R. Buettner, Spin Trapping - Electron-Spin-Resonance Parameters of Spin Adducts, Free Radic. Bio. Med. 3 (1987) 259–303. doi:10.1016/s0891-5849(87)80033-3.
[61] M.C.R. Symons, E. Albano, A. Tomasi, T.F. Slater, Radiolysis of tetrachloromethane, J. Chem. Soc. Faraday Trans. 1. 78 (1982) 2205. doi:10.1039/f19827802205.
[62] J.M. Achord, C.L. Hussey, Determination of dissolved oxygen in nonaqueous electrochemical solvents Determination of Dissolved Oxygen in Nonaqueous Electrochemical Solvents, Anal. Chem. 52 (2002) 601–602. doi:10.1021/ac50053a061.
[63] F. Neese, Prediction of molecular properties and molecular spectroscopy with density functional theory: From fundamental theory to exchange-coupling, Coord. Chem. Rev. 253 (2009) 526–563. doi:10.1016/j.ccr.2008.05.014.
[64] P.B. Mccays, E.K. Lai, J.L. Poyer, C.M. Dubose, G. Janzenll, Oxygen- and Carbon-centered Free Radical Formation during Carbon Tetrachloride Metabolism, J. Biol. Chem. 259 (1984) 2135–2143.
[65] R.G. Compton, P.R. Unwin, Channel and tubular electrodes, J. Electroanal. Chem. Interfacial Electrochem. 205 (1986) 1–20. doi:10.1016/0022-0728(86)90219-6.
[66] D.G. Mitchell, G.M. Rosen, M. Tseitlin, B. Symmes, S.S. Eaton, G.R. Eaton, Use of rapid-scan EPR to improve detection sensitivity for spin-trapped radicals, Biophys. J. 105 (2013) 338–342. doi:10.1016/j.bpj.2013.06.005.
[67] D.G. Mitchell, M. Tseitlin, R.W. Quine, V. Meyer, M.E. Newton, A. Schnegg, B. George, S.S. Eaton, G.R. Eaton, X-band rapid-scan EPR of samples with long electron spin relaxation times: A comparison of continuous wave, pulse and rapid-scan EPR, Mol. Phys. 111 (2013) 2664–2673. doi:10.1080/00268976.2013.792959.

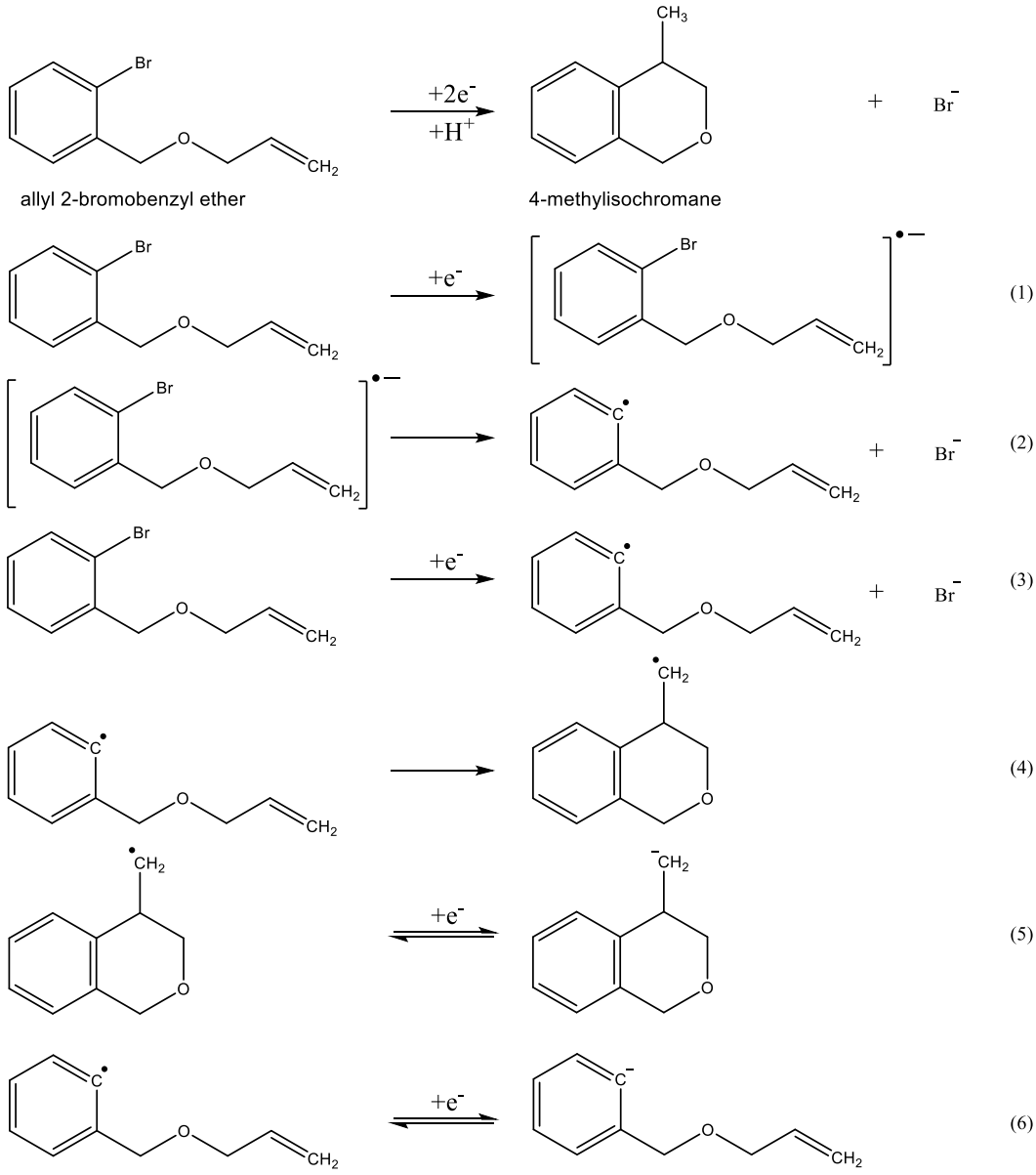

Figure 1: Possible reaction pathways to construct fused aromatic molecules starting from allyl 2-bromobenzyl ether in an aprotic solvent [23].

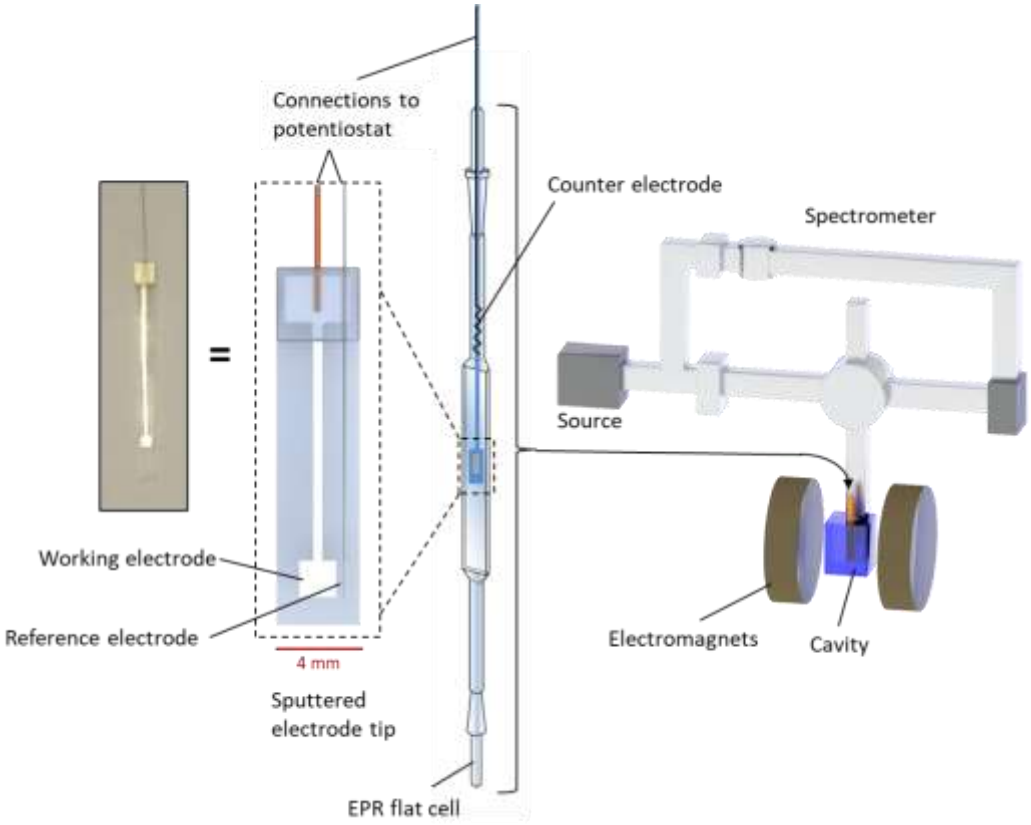

Figure 2: Picture of the electrode tip (left) and schematic illustration of the setup. The electrode tip is positioned in the flat cell which is inserted in the cavity (depicted as a blue box) between the electromagnets of the spectrometer. The orange tube in the cavity represents the flat cell and shows its position.

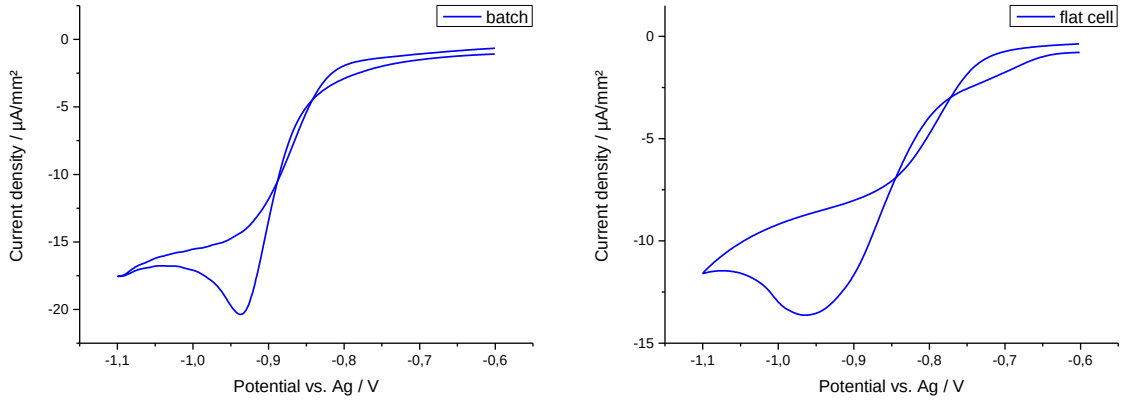

A B

Figure 3: Cyclic voltammetry at 100 mV s^{-1} of 5 mM allyl 2-bromobenzyl ether in ACN + 0.1 M n-Bu_4NClO_4 on an Ag working electrode in a standard batch set-up (A) and in an EPR flat cell (B).

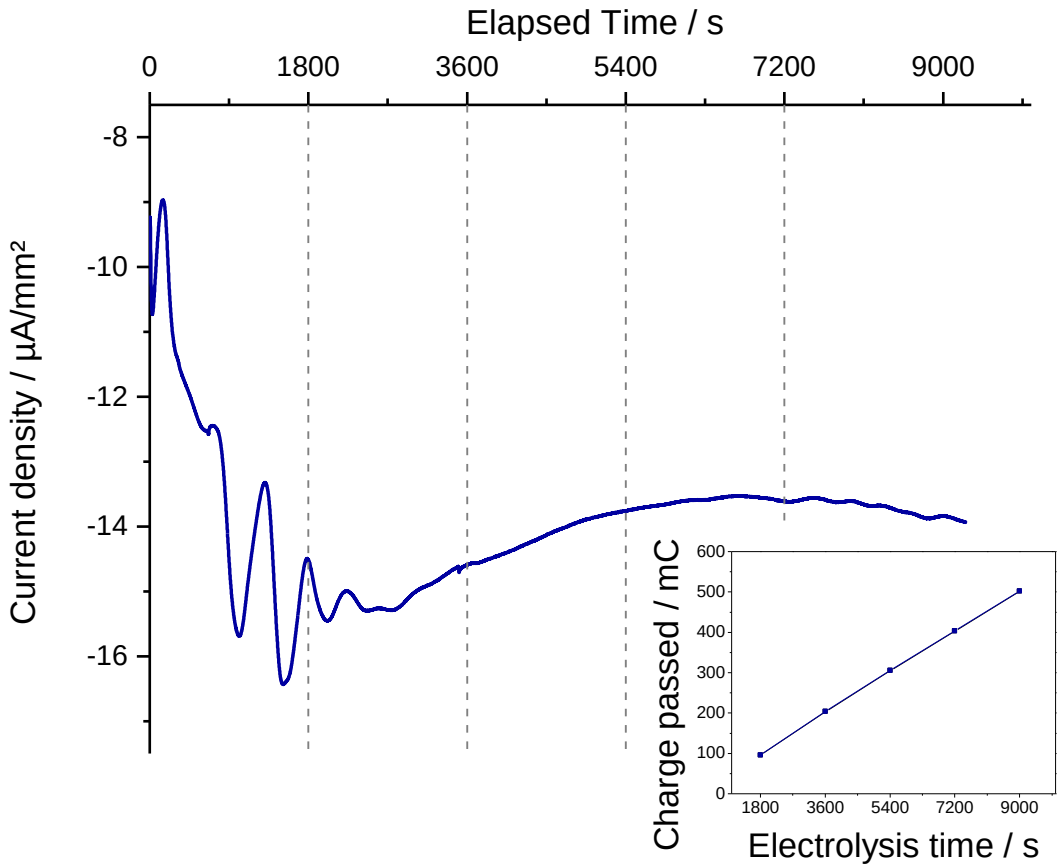

Figure 4: Current response of the potential controlled electrolysis in the EPR flat cell. 4 mm² Ag WE, electrolyte = ACN + 0.1 M TBAP with 5 mM ABBE and 15 mM PBN. The dashed lines mark the 30 min. (20 scan) periods over which the EPR scans are accumulated. Inset: cumulative charge passed during the electrolysis.

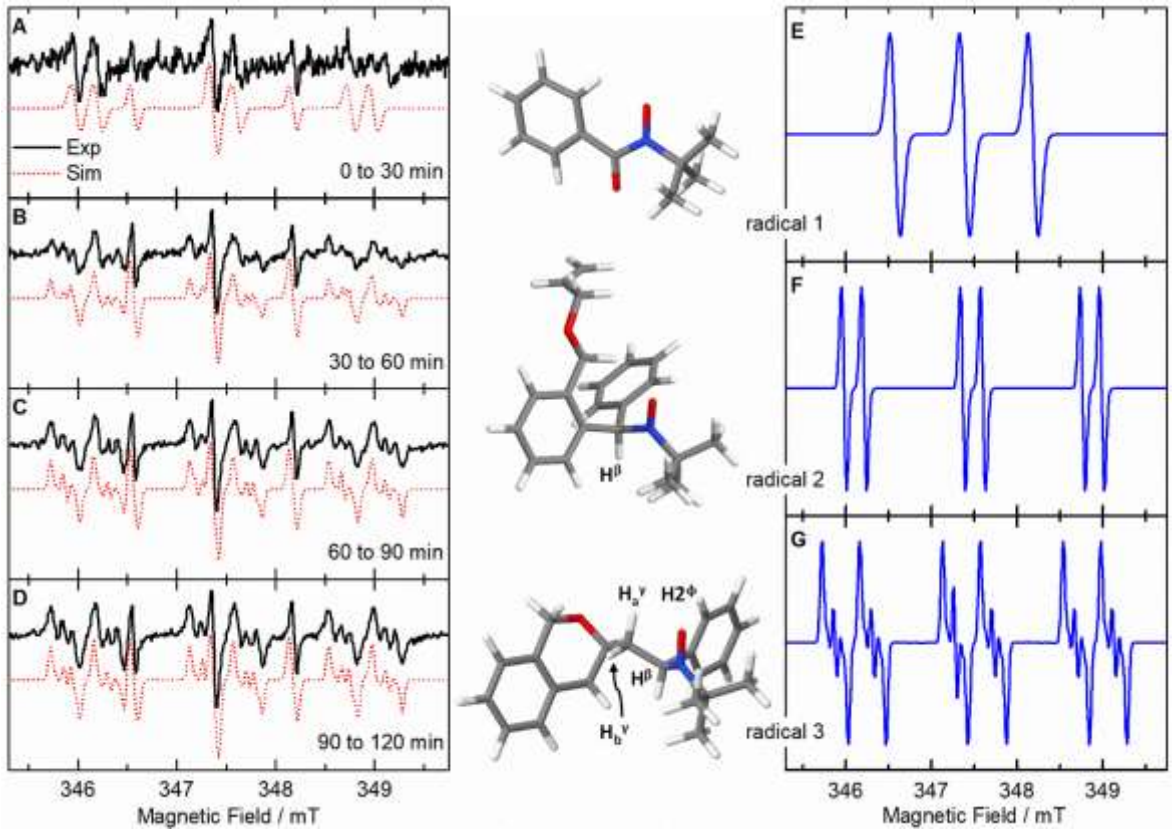

Figure 5: Accumulated experimental EPR spectra (black) and corresponding simulations (red) of the controlled-potential electrolysis of 5 mM ABBE + 15 mM PBN in ACN + 0.1 M TBAP (potential set at the peak potential of the reduction wave in the EPR flat cell, checked by in situ CV) at different time intervals: 0-30 min, (A), 30-60 min (B), 60-90 min (C) and 90-120 min (D), and the simulated spectra and the molecular models derived from DFT calculations of radical 1/PBN-Ox (E), radical 2/PBN-allyl benzyl ether (F) and radical 3/ PBN-4-methylisochromane (G). The spectra are shown normalized to allow easy comparison.

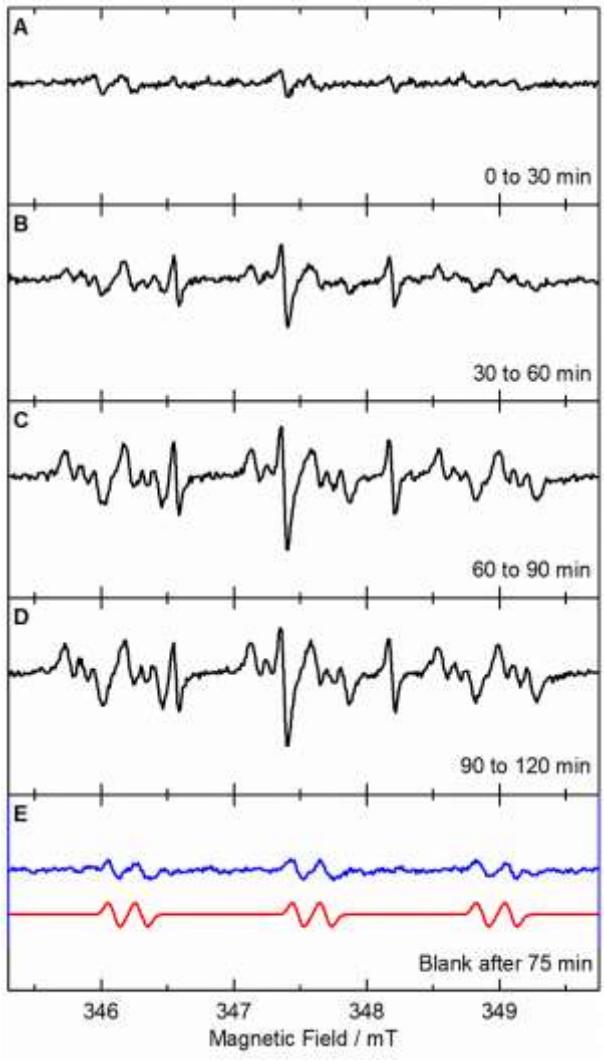

Figure 6: Accumulated experimental EPR spectra (black, 20 scans) of the controlled potential electrolysis of allyl 2-bromobenzyl ether in ACN + 0.1 M TBAP at the peak potential of the reduction wave in the flat cell (-1 V vs. pseudoref.) at different time intervals: 0-30 min, (A), 30-60 min (B), 60-90 min (C) and 90-120 min (D), and the spectrum (blue, 50 scans) and simulation (red) of a sample containing only PBN in ACN with n-Bu4NClO4 collected after 75 min of controlled potential electrolysis at -1V vs. the pseudoref. (E). The parameters for the simulation were giso = 2.0057, AN-iso =39.00 MHz, AH = 5.8 MHz.

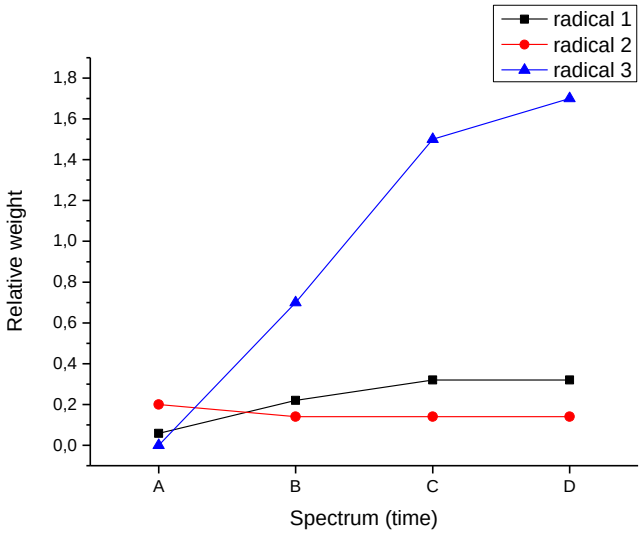

Figure 7: Relative weight of each radical in the different spectra (Figure 5).